PCCP

Biological Control of *S*-Nitrosothiol Reactivity: Potential Role of Sigma-Hole Interactions

Journal:	*Physical Chemistry Chemical Physics*
Manuscript ID	CP-ART-11-2019-006377.R2
Article Type:	Paper
Date Submitted by the Author:	27-Feb-2020
Complete List of Authors:	Hendinejad, Niloufar; Marquette University, Department of Chemistry Timerghazin, Qadir; Marquette University, Department of Chemistry

Received 00th January 20xx,
Accepted 00th January 20xx

DOI: 10.1039/x0xx00000x

Biological Control of *S*-Nitrosothiol Reactivity: Potential Role of Sigma-Hole Interactions

Niloufar Hendinejad[a] and Qadir K. Timerghazin[a]

ABSTRACT: *S*-Nitrosothiols (RSNOs) are ubiquitous biomolecules whose chemistry is tightly controlled in vivo, although the specific molecular mechanisms behind this biological control remain unknown. In this work, we demonstrate, using high-level ab initio and DFT calculations, the ability of RSNOs to participate in intermolecular interactions with electron pair donors/Lewis bases (LBs) via a σ-hole, a region of positive electrostatic potential on the molecular surface at the extension of the N–S bond. Importantly, σ-hole binding is able to modulate the properties of RSNOs by changing the balance between two chemically opposite (antagonistic) resonance components, R–S^{+}=N–O^{-} (***D***) and R–S^{-}/NO^{+} (***I***), which are, in addition to the main resonance structure R–S–N=O, necessary to describe the unusual electronic structure of RSNOs. σ-Hole binding at the sulfur atom of RSNO promotes the resonance structure ***D*** and reduces the resonance structure ***I***, thereby stabilizing the weak N–S bond and making the sulfur atom more electrophilic. On the other hand, increasing the D-character of RSNO by other means (e.g. via *N*- or *O*-coordination of a Lewis acid) in turn enhances the σ-hole bonding. Our calculations suggest that in the protein environment a combination of σ-hole bonding of a negatively charged aminoacid sidechain at the sulfur atom and *N*- or *O*-coordination of a positively charged aminoacid sidechain is expected to have a profound effect on the RSNO electronic structure and reactivity.

1 Introduction

S-Nitrosothiols (RSNOs) are ubiquitous derivatives of nitric oxide, an important biological gasotransmitter.[1] Biological RSNOs derive from small-molecule thiols (glutathione, coenzyme A, and hydrogen sulfide)[2–6] and also cysteine aminoacid side-chains in proteins.[7] *S*-Nitrosation of protein cysteine residues is an important post-translational modification of proteins affecting the protein function, with thousands of proteins already identified to undergo *S*-nitrosation *in vivo*.[8] Besides their role as endogenous biomolecules, RSNOs also have a potential application as NO-producing drugs.[9–12]

Protein *S*-nitrosation is a tightly controlled process *in vivo*, likely mediated through enzymatic reactions;[7,13–15] breakdown of this control has been associated with numerous pathological processes.[16–19] However, the molecular nature of the enzymatic processes behind the RSNO reactions in living organisms remains poorly understood, not in a small degree due to experimental challenges related to the instability of the S–N bond in RSNOs.[20] For instance, only limited number of X-ray structures of *S*-nitrosated proteins is available at the moment.

At the same time, theoretical studies suggest that the reactivity of RSNOs is eminently suitable for enzymatic control. This stems from the unusual antagonistic nature of the RSNO electronic structure:[21–23] proper description of the properties and reactivity of RSNOs requires invoking two resonance structures (in addition to the conventional/main resonance structure ***S***, Chart 1) referred to as ***D*** and ***I***, which are chemical opposites of one another in terms of the formal charges and bonding patterns—*antagonistic* structures. While ***D*** implies a double S=N bond and positively charged sulfur atom and negatively charged oxygen atom, structure ***I*** implies no covalent bonding between S and N atoms and negatively charged sulfur atom and positively charged NO moiety (Chart 1).

The antagonistic model of the RSNO electronic structure reconciles the contradictory properties of the –SNO group,[24,25] i.e. unusually long (~1.8 Å) and weak (dissociation energy ~30 kcal/mol) S–N bond[26–30] and, at the same time, restricted rotation around the S–N bond (the interconversion barrier of *cis*- and *trans*-RSNO conformers >10 kcal/mol).[24,25,30]

[a] *Department of Chemistry, Marquette University, P. O. Box 1881, Milwaukee, Wisconsin 53201-1881, United States.*
E-mail: qadir.timerghazin@marquette.edu

†Electronic Supplementary Information (ESI) available: Supporting figures and tables, Cartesian coordinates and electronic energies for all calculated structures. See DOI: 10.1039/x0xx00000x

Chart 1 Resonance Representation of the RSNO Electronic Structure: The Conventional (***S***) and Antagonistic (***I*** and ***D***) Structures that Promote Opposite Reactivity toward Nucleophiles

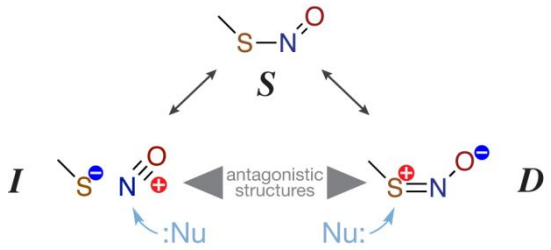

The antagonistic nature of the –SNO group explains the dual reactivity of RSNOs with nucleophiles, e.g. thiols (Chart 1),[31–33] successfully predicts the modulation of the S–N bond properties and RSNO reactivity by external electric fields,[21,30] rationalizes the counterintuitive effects of aromatic substitution in RSNOs,[34] and can be used to predict hitherto unknown reactions of RSNOs.[32]

Importantly, as evident from Chart 2, the antagonistic model also suggests that relative contributions of the RSNO antagonistic resonance structures (and hence the reactivity of RSNOs) can be manipulated by interaction with electron-poor (charged or neutral Lewis acids, LAs) or electron-rich (charged or neutral Lewis bases, LBs) species. Indeed, LA coordination at the O or N atoms of the –SNO group leads to dramatic shortening and strengthening of the S–N bond and activation of the S atom in the reactions with nucleophiles, which is consistent with promotion of the resonance structure ***D*** (Chart 2, top right).[31,32,35] On the other hand, LA coordination at the S atom leads to destabilization of the S–N bond and activation of the NO group in reactions with nucleophiles, which is consistent with promotion of the resonance structure ***I*** (Chart 2, top left).[36,37] These effects of LA coordination on the RSNO structure and reactivity are relatively well understood and have been observed computationally and experimentally for a variety of RSNO-LA complexes.[32,35–43]

Chart 2 External modulation of the RSNO electronic structure

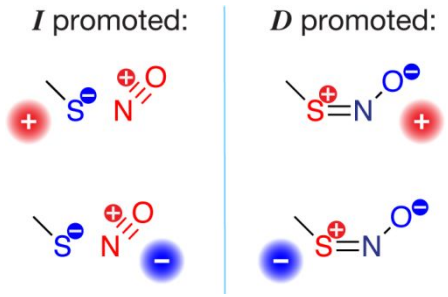

Just like LA coordination can lead to profound changes in the –SNO group, interaction with electron-rich LBs (anionic or neutral) should be able to exert similar (but opposite in effect) control over the RSNO properties (Chart 2, bottom). But, unlike LAs that can easily coordinate to the electron-rich atoms of the –SNO group, coordination of LBs to the –SNO group may seem implausible. However, there is a growing understanding that electron-rich atoms may act as electron pair acceptors thanks to the phenomenon of σ-hole bonding.[44]

σ-Hole is a region of of lower electron density—usually associated with a region of positive electrostatic potential—on the surface of an electron-rich atom at the extension of a polar covalent bond, collinear with that bond.[45–51] In a simplified picture, a σ-hole forms when a *p*-type orbital becomes polarized upon formation of a σ-bond (Fig. 1A). Most often, σ-holes are observed at halogen or chalcogen atoms (Fig. 1B), and the interactions of these σ-holes with LBs are usually referred to as halogen[52] and chalcogen[53] bonding, or σ-hole bonding in general. There is a significant emergent interest in these interactions due their importance for the biological systems[54–63] and materials.[62–67]

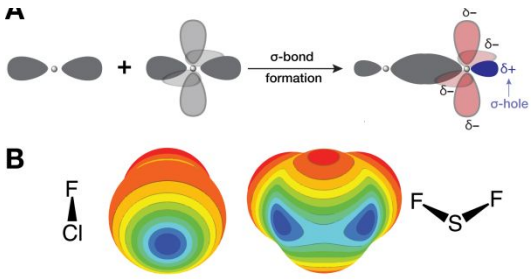

Fig. 1 A σ-hole forms due to polarization of a *p* orbital upon formation of a σ-bond (**A**). Examples of σ-holes (blue) on the molecular surfaces of halogen (chlorine) and chalcogen (sulfur) atoms (**B**).

Interactions of RSNOs with LAs could be one of the main mechanisms of the biological enzymatic control of RSNO reactions.[7,17] The ability of the –SNO group to be involved in σ-hole interactions can provide an additional mechanism for fine-tuning the reactivity of RSNOs, with important implications not only for our understanding of the RSNO biochemistry and the related physiological processes, but also to the design of novel RSNOs of pharmacological interest.[9] This calls for a much better understanding of RSNOs as potential σ-hole donors. Here, we report a detailed computational investigation of the ability of RSNOs to engage in σ-hole/chalcogen bonding, with specific emphasis on how the σ-hole bonding and the electronic structure of the –SNO group affect each other.

2 Computational details

Ab initio calculations were performed with Molpro 2015.1 program package.[68,69] Molecular electrostatic potential of CH_3SNO molecule was calculated using internally-contracted multireference configuration interaction[70] (MRCI) for CCSD(T)-F12/VQZ-F12 geometries reported previously.[30] MRCI calculations used complete active space self-consistent field[71,72] (CASSCF) reference wavefunction obtained with 8-electron/6-orbital active space and Dunning's augmented correlation-consistent quadruple-zeta basis set, aug-cc-pVQZ. Complex geometries were fully optimized (using numerical gradients) with density-fitted explicitly-correlated[73] (F12) local[73–75] coupled-cluster method with single, double, and non-

iterative local triple excitations, LCCSD(T)-F12, with the F12-optimized double- and triple-zeta basis sets, cc-pVDZ-F12 and cc-pVTZ-F12. To minimize the basis set superposition error (BSSE) in molecular complex calculations,[76–78] the orbital domains were localized on individual molecules and determined for non-interacting molecules at >50 Å distance; all intermolecular electron pairs were treated at the highest level, and strong and close pairs were coupled.[79,80]

Density functional theory (DFT) calculations with Perdew-Burke-Ernzerhof hybrid functional[81–83] (PBE0) including Grimme's empirical dispersion correction [84,85] with damping[86] (PBE0-D3BJ) were performed with Gaussian 16 package.[87] DFT calculations used a triple zeta basis set by Weigend and Alritchs with diffuse functions by Rappaport and Furche,[88,89] def2-TZVPPD; quadruple-zeta basis set def2-QZVPPD was also tested. Resonance structure weights were calculated with the Natural Resonance Theory (NRT) analysis,[90,91] as implemented in NBO 7.0 code.[92]

3 Results and discussion

3.1 RSNO electrostatic potential in the gas phase

To identify potential σ-holes at the atoms of the –SNO group, we start with examination of the RSNO molecular electrostatic potential (MEP). Since RSNOs present a significant challenge for electronic structure calculations,[28,29] computationally demanding high-level ab initio methods are required for reliable description of the RSNO properties.[93,30] Here, we evaluated the MEP of our primary model RSNO, CH_3SNO, at the MRCI/aug-cc-pVQZ level, based on the equilibrium geometry optimized at the CCSD(T)-F12/VQZ-F12 level reported earlier.[30]

Fig. 1 presents the MEP $V(r)$ of the two CH_3SNO conformers mapped onto the molecular surface (0.001 au isodensity), with the surface MEP minima ($V_{S,min}$) and maxima ($V_{S,max}$) shown as purple and golden dots, respectively; Table 1 lists the electrostatic potential values for the relevant $V_{S,min}$ and $V_{S,max}$ points. Among the MEP extrema pertinent to intermolecular interactions of the –SNO group are $V_{S,min}$ points corresponding to the lone pairs (LP) on the oxygen, nitrogen, and sulfur atoms; these underline the ability of RSNOs to form complexes with LAs coordinated to either of the three atoms of the –SNO group. Judging by the $V_{S,max}$ values, the oxygen and nitrogen atoms are generally more basic (-16 to -20 kcal/mol) than the sulfur atoms (-10 kcal/mol).

Two surface MEP maxima in the vicinity of the sulfur atom have characteristics of σ-holes. The $V_{S,max}$ point located at the extension of the C–S bond, σH(C-S), is small in magnitude (6 and 3 kcal/mol in *cis*- and *trans*-CH_3SNO, respectively), which is expected considering the low polarity of the C-S bond. On the other hand, $V_{S,max}$ point located at the extension of the N–S bond, assigned as another σ-hole, σH(N-S), is much more prominent (18 kcal/mol). Both σ-holes are not exactly collinear with the corresponding C–S or N–S bonds, i.e. the N(C)–S–σH angles are deviating from 180°, especially in the case of σH(N-S) which appears to be influenced in part by the electrostatic potential created by the methyl group (deviation of 15° for *cis*- and 23° for *trans*-CH_3SNO).

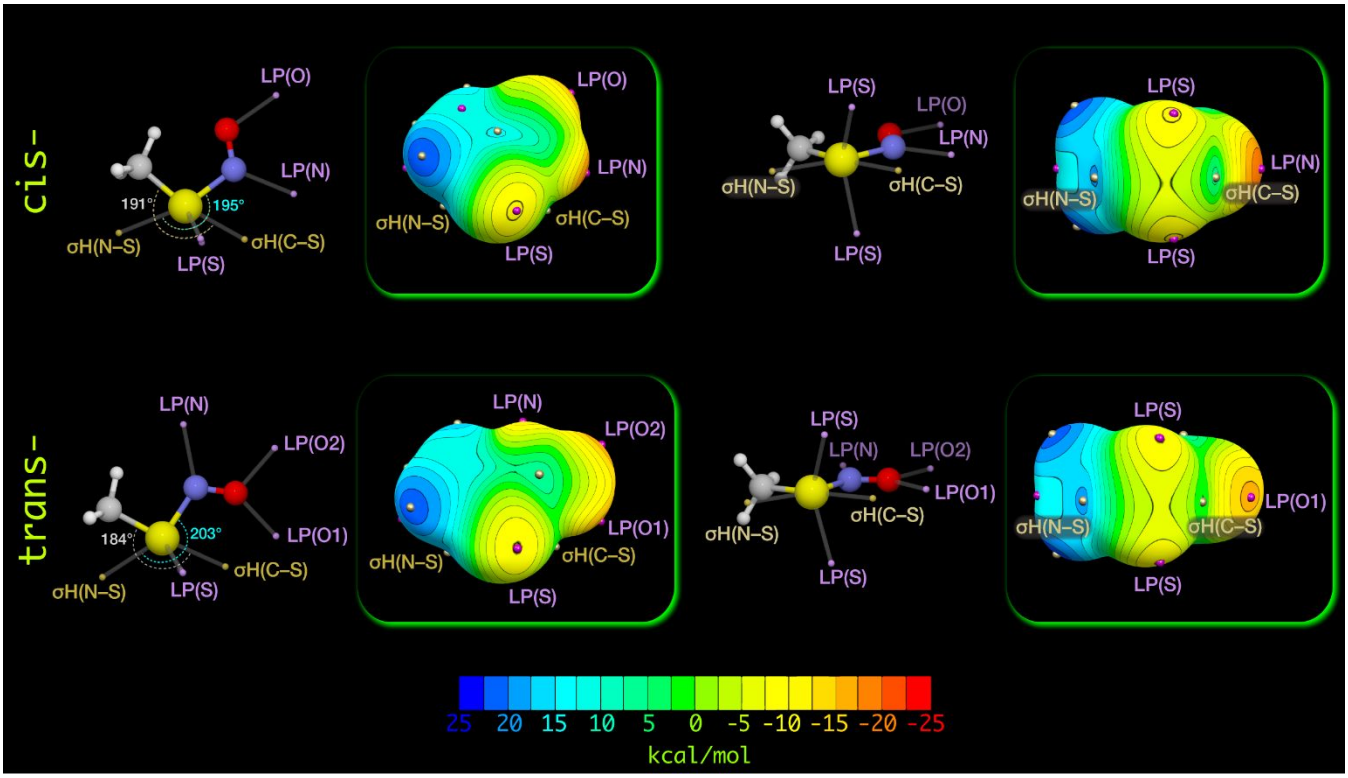

Fig. 2 Top and side views of the molecular electrostatic potential (MEP) of cis- and trans-CH_3SNO calculated at the MRCI/aug-cc-pVQZ level mapped onto the electron density isosurface (0.001 au). Surface MEP minima ($V_{S,min}$) and maxima ($V_{S,max}$) are shown as purple and golden dots, respectively. Reference molecular geometries with relevant $V_{S,min}$ and $V_{S,max}$ points are shown left of the corresponding MEP maps.

Since high-level ab initio calculations are not practical for larger RSNOs/RSNO complexes, it is important to assess the performance of the density functional theory (DFT) methods with respect of reproducing RSNO MEP. Here, we used dispersion-corrected Perdew-Burke-Ernzerhof hybrid density functional with triple-zeta quality basis set, PBE0-D3BJ/def2-TZVPPD, a model chemistry that has been successfully used for modeling of RSNOs and their reactions.[31,93 ,34,22] We find that DFT description of the surface MEP of CH_3SNO conformers (Fig. S1 in ESI) is very similar to that of MRCI/aug-cc-pVQZ (Fig. 1); quantitatively, PBE0-D3BJ/def2-TZVPPD underestimates the magnitude of σH(N-S) by 2 kcal/mol (Table 1), while overestimating the magnitude of LP(O) by 1 kcal/mol and underestimating the magnitude of LP(S) by 2-3 kcal/mol.

Table 1 The maximum and minimum electrostatic potential values on the surface of the sulfur, oxygen and nitrogen atoms in *cis*- and *trans*-CH_3SNO.

$V_{S,min}$ / $V_{S,max}$	MRCI	PBE0	PBE0, short N–S	PBE0-PCM
cis-CH_3SNO				
σH(N-S)	+18	+16	+22	+21
σH(C-S)	+6	+5	+5	+3
LP(O)	-17	-18	-26	-23
LP(N)	-20	-19	-22	-23
LP(S)	-10	-8	-4	-8
trans-CH_3SNO				
σH(N-S)	+18	+16	+22	+21
σH(C-S)	+3	+3	+1	-0.5
LP(O1)	-16	-17	-23	-22
LP(O2)	-18	-19	-27	-24
LP(N)	-13	-12	-18	-15
LP(S)	-10	-7	-3	-7

3.2 σ-Hole bound RSNO complexes in the gas phase

The analysis of the surface MEP suggests that the S atom of the –SNO group can potentially coordinate LBs via interactions with two σ-holes, i.e. give rise to chalcogen bonding. To verify this hypothesis, we used local explicitly-correlated (F12) coupled cluster method with single, double, and perturbative triple excitations, LCCSD(T)-F12, to optimize CH_3SNO complexes with model neutral (formaldehyde) and anionic (acetate ion) electron pair donors. Although the standard coupled cluster methods, e.g. CCSD(T), demonstrate very slow convergence of the calculated properties of the –SNO group,[28,36] and also suffer from large basis set superposition errors (BSSE) when applied to intermolecular complexes, explicitly-correlated methods demonstrate much faster basis set convergence, while local correlation methods can virtually eliminate the BSSE (see Computational Details section). This allows obtaining reliable properties of the RSNO complexes using relatively small one-electron basis sets. Indeed, the σ-hole bound complex geometries and binding energies obtained with a double-zeta basis set, LCCSD(T)-F12/VDZ-F12, differ negligibly from the triple-zeta results, LCCSD(T)-F12/VTZ-F12. Therefore, we further used LCCSD(T)-F12/VDZ-F12 level of theory, which allowed full optimization of fairly large intermolecular complexes.[94]

We were able to optimize complexes with the electron pair donors coordinated collinearly at the extension of the N–S and C–S bonds (Fig. 2). Consistent with the magnitude of the corresponding σ-holes, σH(N–S) and σH(C–S), the complexes formed along the N–S bond ("N-S complexes") are more strongly bound than the complexes formed along the C–S bond ("C-S complexes"); the difference is particularly stark for the acetate complexes, where the N–S complexes have almost four-fold larger binding energies. In the case of the formaldehyde complexes, weak hydrogen bonding involving the C–H bond provides additional stabilization, so the N-S and C-S complexes have similar binding energies, although the S-N complexes are still more stable.

Complexation of the negatively charged acetate anion along the S–N bond is significantly stronger than neutral formaldehyde molecule (13 vs 3 kcal/mol); as here we are concerned with the electronic effects in σ-hole bonding, we use electronic binding energies, BE. On the other hand, the difference in binding energies of the C-S complexes of acetate and formaldehyde is much smaller (5 vs 2 kcal/mol). Interestingly, the N-S complexes formed by *trans*-CH_3SNO are slightly more stable than the similar complexes of *cis*-CH_3SNO, especially for the acetate complexes, ~1 kcal/mol, which is comparable to the *cis*-trans energy difference in CH_3SNO (~1 kcal/mol,[30] favoring the *cis*-form); in effect, chalcogen bonding along the N–S bond seems to selectively stabilize the *trans*-conformer in these cases.

Both formaldehyde and acetate complexes have the characteristics of σ-hole/chalcogen bound complexes. In fact, the donor oxygen atoms are more collinear to the respective N–S and C–S bonds (1°-10° deviation form 180°) than the corresponding σ-holes (15°-23° deviation, Fig. 2). Complexes of *cis*-CH_3SNO are particularly nearly collinear (1°-5° deviation from 180°). The intermolecular S···O distances are typical for halogen/chalcogen bound complexes (2.6-3.4 Å).

DFT results obtained for the CH_3SNO complexes with formaldehyde and acetate at the PBE0-D3BJ/def2-TZVPPD level (Fig. 2) are in excellent agreement with the LCCSD(T)-F12/VDZ-F12 results both in terms of the binding energies and complex geometries. Interestingly, although DFT slightly underestimates the magnitude of the surface MEP maxima corresponding to the σ-holes, the DFT binding energies of the σ-hole bound complexes are 0.2–0.9 kcal/mol higher, with the exception of the N-S complex of *trans*-CH_3SNO and acetate where the DFT binding energy is 1.8 kcal/mol higher than the LCCSD(T)-F12 value. In terms of the geometries, PBE0-D3BJ/def2-TZVPPD slightly overestimates the intermolecular S···O distances for the complexes with formaldehyde (by <0.1 Å) and underestimates the S···O distances in the complexes with acetate by ~0.1 Å.

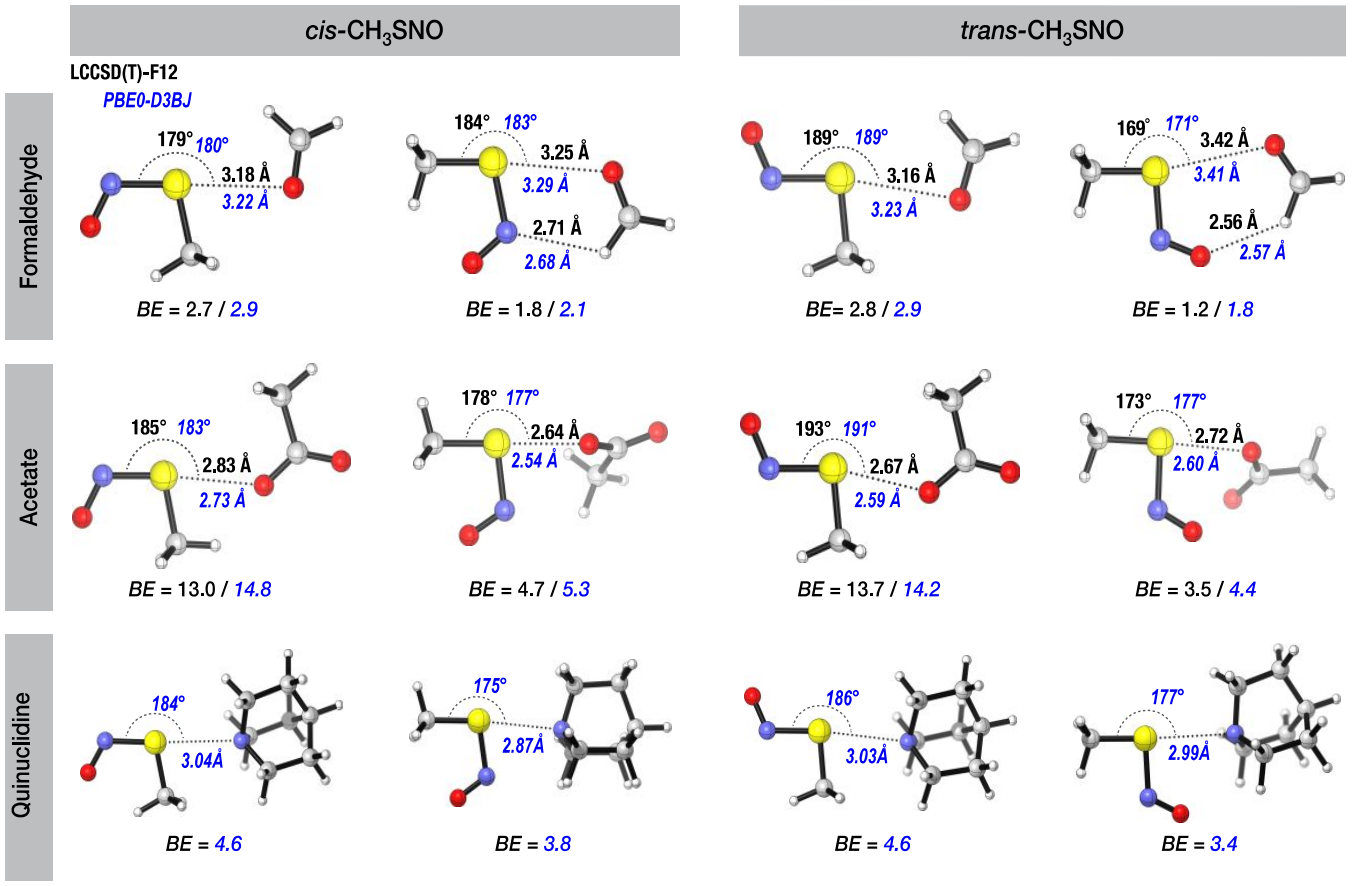

Fig. 3 σ-Hole bound complexes of CH_3SNO with formaldehyde, acetate, and quinuclidine with relevant geometric parameters and binding energies (*BE*) calculated with LCCSD(T)-F12/VDZ-F12 (black typeface) and PBE0-D3BJ/def2-TZVPPD (blue typeface).

To gauge the importance of the BSSE and other basis set incompleteness effects on the DFT calculations, we also performed full optimizations of the CH_3SNO complexes with formaldehyde and acetate with a larger quadruple-zeta quality basis set, def2-QZVPPD, which yielded results just marginally different from def2-TZVPPD (Fig. S3 in ESI). Overall, compared to the high-quality LCCSD(T)-F12 data, DFT calculations with PBE0-D3BJ/def2-TZVPPD model chemistry provide adequate qualitative and quantitative description of the σ-hole bound complexes of RSNOs, and can be used for further investigation of these complexes.

To better understand the difference in σ-hole binding of the neutral vs. charged LBs, we used DFT to probe σ-hole binding of CH_3SNO with a strong neutral electron pair donor, quinuclidine, which also has an advantage of being less prone to secondary hydrogen-bonding compared to formaldehyde. The binding energies in quinuclidine complexes (Fig. 3) are significantly smaller than in the charged-assisted complexes of acetate, but almost twice as large than the formaldehyde complexes, which is also reflected in the shorter S···N interaction distances (~3.0 Å).

Like the acetate complexes, quinuclidine-*cis*-CH_3SNO C-S complex has a shorter S···O distance than the N-S complex (2.87 Å vs 3.04 Å, respectively), despite the smaller binding energy (3.8 kcal/mol vs 4.6 kcal/mol). A similar effect, to a lesser degree, is observed for *trans*-CH_3SNO complexes, where C-S and N-S complexes have almost the same S···N distance (2.99 Å vs 3.03 Å, respectively), although the former has a lower binding energy (3.4 kcal/mol vs 4.6 kcal/mol, respectively).

Thus, the presence of two σ-holes at the sulfur atom of the –SNO group gives rise to two types of σ-hole bound complexes with LBs (neutral and anionic) at the extension of the N–S (stronger complexes) and C–S (weaker complexes) bonds.

3.3 Interrelation between σ-hole bonding and the properties of the –SNO group

The antagonistic model of the RSNO electronic structure suggests that the coordination of a LB at the sulfur atom of the –SNO group should favor higher contribution from the zwitterionic resonance structure ***D*** and reduce the contribution from the ionic resonance structure ***I*** (Chart 2). As a consequence, the S–N bond should become stronger and shorter and the sulfur atom more electrophilic which in turn should enhance the σ-hole bonding. Here, we discuss the effect of σ-hole binding on the properties of the –SNO group using acetate and quinuclidine as model LBs, since the effect of formaldehyde coordination is confounded by the secondary hydrogen bonding interactions.

As expected, formation of these complexes leads to shortening of the S–N bond (Table 2) consistent with increasing contribution of the zwitterionic resonance structure ***D***. Given the technical difficulties with obtaining consistent NRT description of larger intermolecular complexes, here we gauge the balance

Table 2 . The S–N bond lengths and bond length changes upon complexation (in Å) in σ-hole bound CH_3SNO complexes; PBE0-D3BJ/def2-TZVPPD calculations.

	BH_3 at O or N	N-S or C-S	r(S-N)	Δr(S-N)
cis-CH_3SNO			1.779	
cis-CH_3SNO-quinuclidine		N-S	1.754	-0.025
cis-CH_3SNO-acetate		N-S	1.701	-0.078
cis-CH_3SNO-quinuclidine		C-S	1.765	-0.014
cis-CH_3SNO-acetate		C-S	1.749	-0.030
trans-CH_3SNO			1.789	
trans-CH_3SNO-quinuclidine		N-S	1.770	-0.019
trans-CH_3SNO-acetate		N-S	1.728	-0.061
trans-CH_3SNO-quinuclidine		C-S	1.798	+0.019
trans-CH_3SNO-acetate		C-S	1.812	+0.023
cis-CH_3SNO-BH_3	O		1.654	-0.125
cis-CH_3SNO-BH_3-quinuclidine	O	N-S	1.651	-0.128
cis-CH_3SNO-BH_3-acetate	O	N-S	1.641	-0.138
cis-CH_3SNO-BH_3-quinuclidine	O	C-S	1.655	-0.124
cis-CH_3SNO-BH_3-acetate	O	C-S	1.650	-0.129
cis-CH_3SNO-BH_3	N		1.713	-0.066
cis-CH_3SNO-BH_3-quinuclidine	N	N-S	1.713	-0.066
cis-CH_3SNO-BH_3-acetate	N	N-S	1.715	-0.064

between ***D*** and ***I*** structures by the variation of the S–N bond length, which we demonstrated be an excellent metric to describe the ***D***- vs ***I***-character of the –SNO group.[22]

Consistent with the larger binding energies, the acetate binding has a significant effect on the S–N bond shortening/strengthening and increase of its double-bond character, although quinuclidine binding also leads to sizable changes in the S–N bond properties (Table 2). The effect is slightly smaller in the case of the S-N complexes of *trans*-CH_3SNO compared to *cis*-CH_3SNO, despite similar binding energies.

In the case of the C-S complexes, there is a significant difference in how the LB binding affects the S–N bond in *cis*- and *trans*-CH_3SNO complexes. The C-S complexes of *cis*-CH_3SNO demonstrate similar (but smaller in scale) effect as the S-N complexes: the S–N bond becomes stronger. However, in the case of *trans*-CH_3SNO the effect is opposite: the S–N bond becomes longer. In terms of the antagonistic model, this weakening of the S–N bond upon the C–S binding of a LB to *trans*-CH_3SNO originates from the interaction of the LB with the NO moiety which promotes the ionic structure ***I*** (Chart 2).

Thus, interaction of a LB with sulfur atom of the –SNO group promotes the zwitterionic resonance structure ***D*** and decreases the contribution of the ionic resonance structure ***I*** (except in the special case of the C-S complexes of *trans*-CH_3SNO). At the same time, increasing the ***D*** character by some other means is expected to lead to stronger σ-hole binding by increasing the electrophilic character of the S atom. To test this hypothesis, we considered *S*-binding of LBs (acetate and quinuclidine) to CH_3SNO with a LA (BH_3) coordinated at the O or N atoms of the –SNO group.

Although the molecular surface minima of the ESP, $V_{S,max}$, values are not vastly different for the oxygen and nitrogen atoms of *cis*-CH_3SNO at the PBE0 level (-18 vs -19 kcal/mol, Table 1), the nitrogen atom has a much higher affinity to BH_3 compared to the oxygen atom (31 kcal/mol vs 16 kcal/mol, respectively; Fig. 4). In both cases, BH_3 coordination has a profound effect on the –SNO group electronic structure: by selectively promoting the structure ***D***, the LA binding leads to a dramatic shortening of the S–N bond (by 0.07-0.13 Å, Table 2). The effect is particularly strong in the case of the coordination at the oxygen atom which not only disfavors the ionic structure ***I***, but also strongly promotes the zwitterionic structure ***D*** (Chart 2).

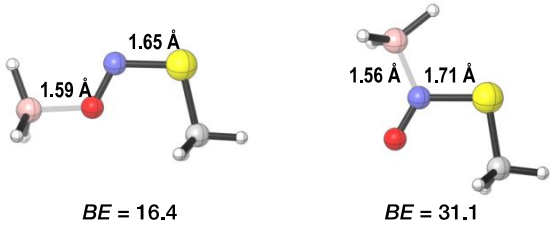

Fig. 4 *O*- and *N*-coordinated complexes of BH_3 with *cis*-CH_3SNO with relevant geometric parameters and binding energies (*BE*) calculated with PBE0-D3BJ/def2-TZVPPD.

The profound changes of the –SNO group electronic structure upon LA coordination at the oxygen or nitrogen atoms that result in promotion of the resonance structure ***D*** lead to significant enhancement of the σ-hole binding at the sulfur atom. There is a roughly two-fold increase in the binding energy of the LBs to the

O-coordinated *cis*-CH_3SNO-BH_3 complex (Figs. 5 vs 3, and Table S4 in ESI). The intermolecular S···O and S···N distances shorten by ~0.3 Å and ~0.15 Å for the acetate and quinuclidine complexes, respectively (Table 2).

BH_3 coordination at the nitrogen atom has even stronger effect on the intermolecular S···O and S···N interactions (shortening of ~0.4 Å for acetate and ~0.2 Å for quinuclidine). The C-S complexes with O-coordinated BH_3 show enhancements of the intermolecular bonding similar to the N-S complexes; however, due to the steric repulsion between the BH_3 and the LB moieties, ternary complexes with *N*-coordinated BH_3 could not be located.

Importantly, binding of a LB at the sulfur atom also enhances the binding of a LA (BH_3). This effect is particularly strong in the case of the acetate complex where the *O*-coordinated BH_3 binding energy increases from 16.4 kcal/mol to 30.7 kcal/mol in the case of the S–N complexes; for quinuclidine complexes the effect is less dramatic but still significant (16.4 kcal/mol to 19.4 kcal/mol). At the same time, the corresponding B–O/B–N bond shortening due to a LB binding is relatively small (0.017- 0.004 Å).

To disentangle the effects of the specific LA (BH_3) and analyze the effect of the increase of the ***D*** character of the RSNO electronic structure on the σ-hole binding, we have considered the σ-hole binding ability of the *cis*-CH_3SNO with the S–N bond artificially shortened to 1.65 Å. As observed previously,[37] shortening of the S–N bond increases the contribution of the resonance structure ***D*** (25% to 32%, Fig. S4 in ESI), and decreases the contribution of the structure ***I*** (16% to 11%). The increased ***D*** character of *cis*-CH_3SNO upon shortening of the S–N bond to 1.65 Å is in agreement with the changes of the surface electrostatic potential (Table 1): the oxygen atom becomes significantly more basic [LP(O) value increases from -18 kcal/mol to -26 kcal/mol], the sulfur atom becomes more electrophilic at the N-S σ-hole [σH(N-S) value increases from 16 kcal/mol to 2 kcal/mol] while losing its basicity at the lone pair [LP(S) value decreases from -8 kcal/mol to -4 kcal/mol].

As expected, shortening of the S–N bond leads to stronger binding of the LBs, in particular in the case of the N-S complexes: by 1.5 kcal/mol for the acetate complex, and 0.5 kcal/mol for the quinuclidine complex (Fig. S5 in ESI vs Fig. 3). The much weaker effect of the S–N bond shortening compared to *O*- and *N*-coordination of a LA is expected, as the latter results in a more significant suppression of the ***I***-character of CH_3SNO (5% in *O*-coordinated *cis*-CH_3SNO-BH_3 complex vs 11% in *cis*-CH_3SNO with a shortened S–N bond), although the ***D***-character is similar in both cases (~30%).

To conclude, there is an important interrelation between the σ-hole binding and the degree of ***D***-character of RSNOs: σ-hole binding of a LA promotes ***D***-character of the –SNO group, and, at the same time, increasing the ***D***-character of the –SNO group enhances the σ-hole binding. A consequence of this interrelation is a strong cooperativity of *O*- or *N*-coordination of a LA and *S*-coordination of a LB to a RSNO molecule.

3.4 Polarizable environment effects on the RSNO electrostatic Potential and σ-hole binding

The σ-hole interactions can have a considerable effect on the RSNO electronic structure (and hence the reactivity), as demonstrated by the ab initio and DFT calculations in the gas phase discussed above. However, in the biological context, these interactions can be affected by environment; thus, to assess the effect of non-specific solvent effects on RSNO σ-hole interactions, we used polarizable continuum model (PCM) with ε=4.2 (corresponding to diethylether solvent) commonly employed to model protein environment.

Transition to a polarizable environment modifies the surface MEP features of CH_3SNO. The σ-hole at the extension of the S–N bond, σH(N-S), becomes more prominent, increasing from 16

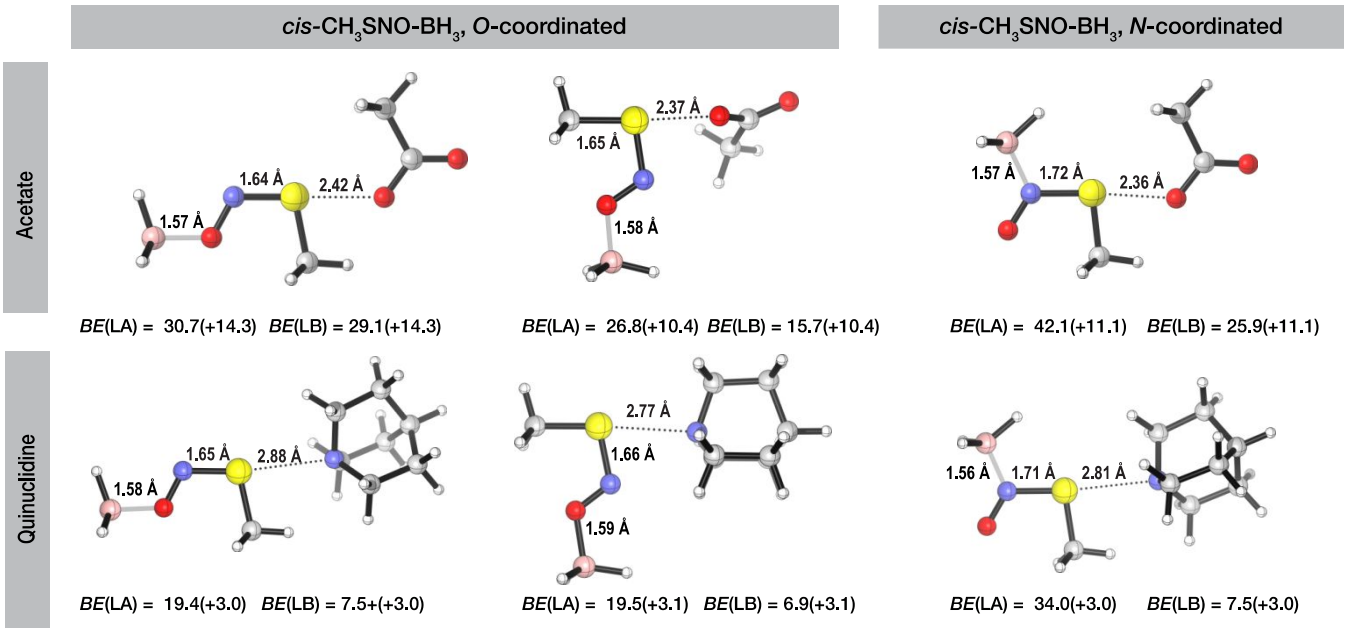

Fig. 5 σ-Hole bound ternary complexes of CH_3SNO with acetate, and quinuclidine as LB and borane as Lewis acid (LA) with relevant geometric parameters and binding energies (*BE*) calculated with PBE0-D3BJ/def2-TZVPPD in the gas phase. The values in parenthesis indicate binding energy enhancements relative to the corresponding binary complexes.

kcal/mol in the gas phase to 21 kcal/mol (Table 1); at the same time, σH(C-S) becomes weaker (>5 kcal/mol to 3 kcal/mol). Basicity of the sulfur atom does not significantly change [-8 kcal/mol for LP(S)], while the basicity of the oxygen and nitrogen atoms increases by ~4 kcal/mol [-23 kcal/mol for LP(O) and LP(N)].

Although the binding energies of the intermolecular complexes are expected to decrease going from vacuum to polarizable environment, the more prominent σH(N-S) partially compensates this effect. Indeed, the binding energy of the quinuclidine N-S complex is only slightly smaller than in the gas phase (4 kcal/mol vs 5 kcal/mol, Fig. S6 in ESI). However, binding of the negatively charged acetate is reduced from 14.8 kcal/mol in vacuum to 4.3 kcal/mol (the CH_3SNO-acetate interaction in polarizable environment is discussed in detail in the following section). In accord with the weakening of the C-S σ-hole in the polarizable environment, quinuclidine C-S complex becomes weaker (<3 kcal/mol, Fig. S6 in ESI), and in the case of acetate we were not able to locate a stable C-S complex.

In the ternary complexes with quinuclidine and BH_3, the quinuclidine binding energy (~7 kcal/mol for N-S complexes) and the enhancement of the binding energies (~3 kcal/mol) do not significantly change upon transition to polarizable environment. In the case of the ternary complexes with acetate and BH_3, the polarizable environment decreases acetate binding energies by >15 kcal/mol, although they remain quite substantial (>10 kcal/mol); the binding energy enhancements also decrease roughly by half (6-7 kcal/mol, Fig. S7 in ESI).

Polarizable environment boosts BH_3 binding to CH_3SNO in the binary complexes and CH_3SNO/quinuclidine ternary complexes by 4 and 2 kcal/mol for *O*- and *N*-coordinated BH_3, which is consistent with increased basicity of O and N atoms in CH_3SNO. On the other hand, compared to vacuum, the BH_3 binding energy decreases in ternary complexes with CH_3SNO/acetate by ~5 kcal/mol.

To conclude, the polarizable environment does not significantly affect σ-hole binding of neutral LBs at the extension of the N–S bond, while attenuating the binding of negatively charged LBs, although the binding energies still remain substantial (>10 kcal/mol). At the same time, the C-S σ-hole bound complexes become less important, in particular, in the case of negatively charged LBs.

3.5 RSNO σ-hole binding in the biological context

As the σ-hole interactions of RSNOs with neutral and negatively charged LBs appear to be able to survive in a polarizable environment similar to a protein setting, we next use PBE0-D3BJ-PCM(ε=4.2)/def2-TZVPPD calculations to investigate potential σ-hole interactions of RSNO with LBs and LB/LA pairs that can be encountered within proteins using truncated models of acidic and basic aminoacid side chains (for brevity, we use the aminoacid codes to refer to the truncated models of the corresponding aminoacid sidechains). To better estimate the actual strength of the intermolecular interactions in the biological environment, from hereon we consider the complex binding enthalpies (*BH*) instead of the electronic binding energies (*BE*) which we used to discuss the nature of the intermolecular interactions in preceding sections.

In terms of negatively charged LBs, we examine deprotonated sidechains of aspartic (Asp^-) and glutamic (Glu^-) acids represented by acetate anion as a truncated model (we already presented a detailed discussion of acetate-RSNO binding in

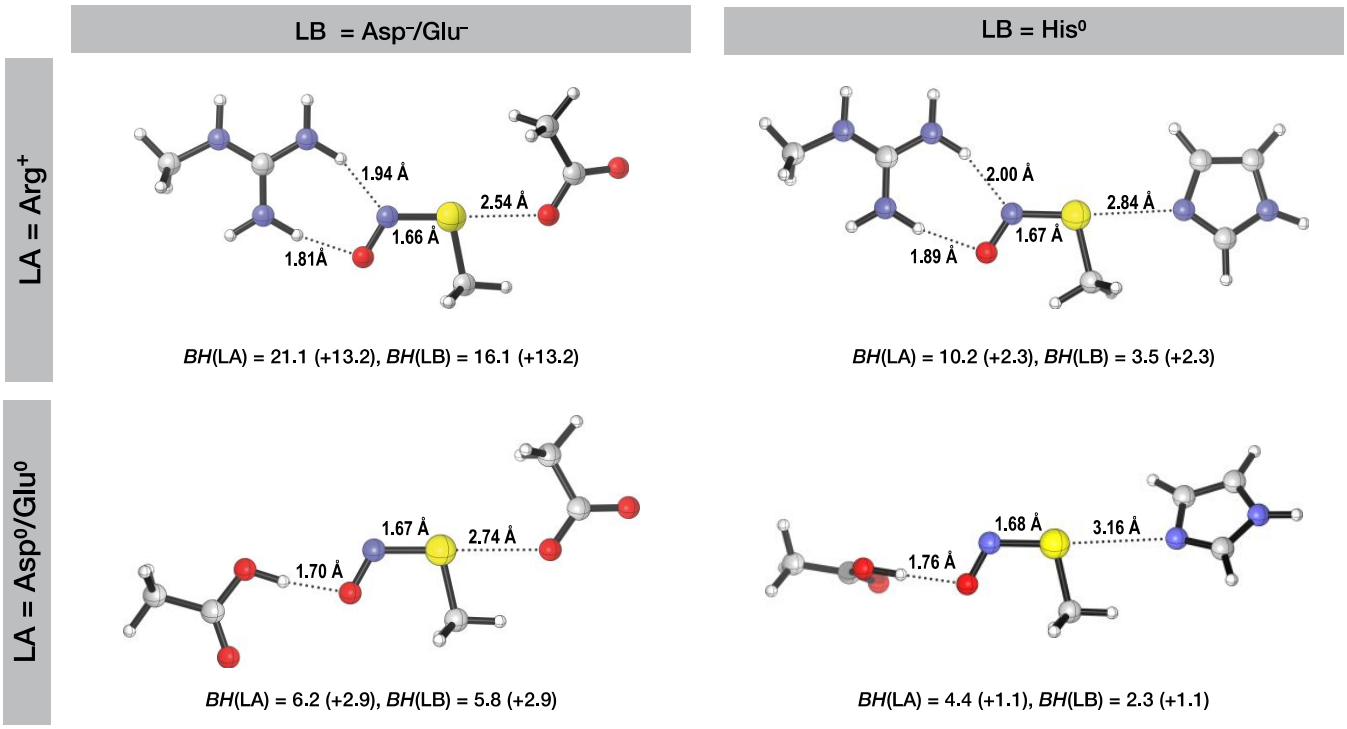

Fig. 6 Representative σ-hole bound ternary complexes of *cis*-CH_3SNO with models of charged and neutral aminoacid side chains with relevant geometric parameters and binding enthalpies (*BH*) calculated with PBE0-D3BJ-PCM(ε=4.2)/def2-TZVPPD. The values in parenthesis indicate binding enthalpy enhancements relative to the corresponding binary complexes. All model complexes calculated are presented in Figs. S10 and S11 (in ESI).

vacuum in previous sections). As a neutral base, we consider histidine (His^0) aminoacid side chain model, which is more likely to stay unprotonated compared to other basic side chains ($pK_a \sim 6$).

Neutral His^0 is able to form a σ-hole bound N–S complexes with *cis*- and *trans*-CH_3SNO (Fig. S8 and Table S8 in ESI), which are expectedly less stable than the analogous complexes with $Asp^–$/$Glu^–$ (*BH* 1.2 kcal/mol vs 3 kcal/mol, respectively); there is an appreciable shortening of the S–N bond due to His^0 coordination (0.026 Å for *cis*- and 0.022 Å for *trans*-CH_3SNO), although the $Asp^–$/$Glu^–$ coordination effect is twice as much (0.052 Å and 0.040 Å).

As LAs that can bind to oxygen and nitrogen atoms of the –SNO group in the protein environment, we consider models of protonated side chains of lysine (Lys^+), arginine (Arg^+), and histidine (His^+), as well as a model of neutral aspartic/glutamic acid side chains (Asp^0/Glu^0).

Charged basic residue models form fairly strong hydrogen bonds with the oxygen and nitrogen atoms of the –SNO group (7-8 kcal/mol), also leading to significant shortening of the S–N bond (0.06-0.09 Å, Fig. S9 and Table S9 in ESI) due to promotion of the ***D*** resonance component. Compared to the positively charged side chains, the hydrogen bonding between the –OH groups of neutral Asp^0/Glu^0 and the oxygen and nitrogen atoms of the –SNO group is two times weaker (3-4 kcal/mol), with still a substantial effect on the S–N bond (0.05-0.07 Å shortening).

Overall, we were able to optimize structures for 25 ternary *cis*- and *trans*-CH_3SNO complexes with aminoacid side chain models (Fig. 6 and Figs. S10-S11 in ESI), with *O*- or/and *N*-coordinated LA (Lys^+, Arg^+, His^+ or Asp^0/Glu^0) and *S*-coordinated LB (His^0 or $Asp^–$/$Glu^–$). Arg^+ complexes involved simultaneous *O*- and *N*-coordination, whereas in the case of *cis*-CH_3SNO, some complexes with *N*-coordinated LA could not be obtained due to formation of a direct hydrogen bond between the acid and the base (Fig. S10).

In the case of both LA and LB being charged, the LA/LB binding enthalpy enhancement is significant, ~13 kcal/mol, while for the complexes with charged LAs and neutral His^0 as the LB the enhancement is an order of magnitude smaller, 2-3 kcal/mol, and in case of both LA and LB being neutral the enhancement is no more than 1 kcal/mol. Strengthening of the σ-hole LB binding due to LA coordination is also evident by contraction of the intermolecular distances by 0.2-0.4 Å. Strengthening of the intermolecular hydrogen bonding of LAs to CH_3SNO is more modest, 0.02-0.1 Å. Importantly, the synergistic effect of the simultaneous LA and LB coordination to the –SNO group results in significant overall strengthening of the S–N bond evidenced by its overall shortening by 0.07-0.11.

To conclude, in the biological context the σ-hole/chalcogen bonding involving the –SNO group is expected to have most of the impact in combination with hydrogen-bonding of the positively charged basic sidechains at the O or N atoms.

4 Conclusions

In this work, we computationally investigated the ability of the sulfur atom of the *S*-nitrosothiol –SNO group to participate in σ-hole/chalcogen bonding non-covalent interactions. We demonstrated existence of a sufficiently prominent σ-hole at the extension of the N–S bond that can engage in interactions with negatively charged or neutral Lewis bases (LBs). Importantly, a LB coordination at the sulfur atom via the σ-hole promotes the zwitterionic resonance structure ***D*** and reduces the ionic structure ***I*** of RSNO (Chart 1); in turn, increased ***D***-character of the –SNO group improves σ-hole bonding. Thus, Lewis acid (LA) coordination at the oxygen or nitrogen atoms significantly increases ***D***-character and thus strengthens the σ-hole bonding; conversely, LB coordination at the sulfur atom improves the LA-RSNO hydrogen bonding.

To understand the importance of this synergistic effect of LA and LB interactions with the –SNO group in biological context, we investigated a number of possible ternary complexes of RSNOs with truncated models of aminoacid sidechains acting as LAs or LBs. This short survey indicates that, using the basic and acidic aminoacid sidechains in various protonation states, proteins can fine-tune the –SNO group electronic structure, and hence its stability and reactivity. While σ-hole interactions with Lewis bases (deprotonated acidic and unprotonated basic aminoacid sidechains) may have a weaker impact on the –SNO group properties, they can play an important role by enhancing the effect of *O*- or *N*-coordination of charged LAs (protonated basic residues). Thus, the biological environment possesses a versatile toolkit to take full advantage of the antagonistic nature of RSNOs to control their reactivity; understanding the molecular details of this control is essential for unraveling the complex mechanisms of physiological and pathological processes involving RSNOs.

ACKNOWLEDGMENT

Q.K.T. is a recipient of the National Science Foundation (NSF) CAREER award CHE-1255641, and Marquette University Way-Klinger Sabbatical Award. This work used the high-performance computing cluster at the Extreme Science and Engineering Discovery Environment (XSEDE) supported by NSF grant ACI-1053575.

References

1 B. C. Smith and M. A. Marletta, *Curr. Opin. Chem. Biol.*, 2012, **16**, 498–506.
2 K. A. Broniowska, A. R. Diers and N. Hogg, *Biochim. Biophys. Acta - Gen. Subj.*, 2013, **1830**, 3173–3181.
3 P. Anand, A. Hausladen, Y.-J. Wang, G.-F. Zhang, C. Stomberski, H. Brunengraber, D. T. Hess and J. S. Stamler, *Proc. Natl. Acad. Sci. U. S. A.*, 2014, **111**, 18572–7.
4 M. R. Filipovic, J. Zivanovic, B. Alvarez and R. Banerjee, *Chem. Rev.*, 2018, **118**, 1253–1337.
5 S. B. King, *Free Radic. Biol. Med.*, 2013, **55**, 1–7.
6 I. Ivanovic-Burmazovic and M. R. Filipovic, *Inorg. Chem.*, 2019, **58**, 4039–4051.
7 C. T. Stomberski, H.-L. Zhou, L. Wang, F. van den Akker and J. S. Stamler, *J. Biol. Chem.*, 2019, **294**, 1568–1578.

8 D. Seth and J. S. Stamler, *Curr. Opin. Chem. Biol.*, 2011, **15**, 129–136.
9 B. Meyer, A. Genoni, A. Boudier, P. Leroy and M. F. Ruiz-Lopez, *J. Phys. Chem. A*, 2016, **120**, 4191–4200.
10 M. Parent, A. Boudier, F. Dupuis, C. Nouvel, A. Sapin, I. Lartaud, J.-L. Six, P. Leroy and P. Maincent, *Eur. J. Pharm. Biopharm.*, 2013, **85**, 640–9.
11 C. Gaucher, A. Boudier, F. Dahboul, M. Parent and P. Leroy, *Curr. Pharm. Des.*, 2013, **19**, 458–72.
12 F. Dahboul, C. Perrin-Sarrado, A. Boudier, I. Lartaud, R. Schneider and P. Leroy, *Eur. J. Pharmacol.*, 2014, **730**, 171–9.
13 C. T. Stomberski, D. T. Hess and J. S. Stamler, *Antioxid. Redox Signal.*, 2019, **30**, 1331–1351.
14 D. Seth, D. T. Hess, A. Hausladen, L. Wang, Y. Wang and J. S. Stamler, *Mol. Cell*, 2018, **69**, 451-464.e6.
15 P. Anand and J. S. Stamler, *J. Mol. Med. (Berl).*, 2012, **90**, 233–44.
16 M. W. Foster, D. T. Hess and J. S. Stamler, *Trends Mol. Med.*, 2009, **15**, 391–404.
17 T. Nakamura, S. Tu, M. W. Akhtar, C. R. Sunico, S. Okamoto and S. A. Lipton, *Neuron*, 2013, **78**, 596–614.
18 M. J. Cutler, B. N. Plummer, X. Wan, Q.-A. Sun, D. Hess, H. Liu, I. Deschenes, D. S. Rosenbaum, J. S. Stamler and K. R. Laurita, *Proc. Natl. Acad. Sci.*, 2012, **109**, 18186–18191.
19 E. Bignon, M. F. Allega, M. Lucchetta, M. Tiberti and E. Papaleo, *Front. Oncol.*, 2018, **8**, 272.
20 E. Bechtold and S. B. King, *Antioxid. Redox Signal.*, 2012, **17**, 981–91.
21 Q. K. Timerghazin and M. R. Talipov, *J. Phys. Chem. Lett.*, 2013, **4**, 1034–1038.
22 M. R. Talipov and Q. K. Timerghazin, *J. Phys. Chem. B*, 2013, **117**, 1827–1837.
23 A. Zeida, C. M. Guardia, P. Lichtig, L. L. Perissinotti, L. A. Defelipe, A. Turjanski, R. Radi, M. Trujillo and D. A. Estrin, *Biophys. Rev.*, 2014, **6**, 27–46.
24 M. D. Bartberger, K. N. Houk, S. C. Powell, J. D. Mannion, K. Y. Lo, J. S. Stamler and E. J. Toone, *J. Am. Chem. Soc.*, 2000, **122**, 5889–5890.
25 N. Arulsamy, D. S. Bohle, J. A. Butt, G. J. Irvine, P. A. Jordan and E. Sagan, *J. Am. Chem. Soc.*, 1999, **121**, 7115–7123.
26 M. D. Bartberger, J. D. Mannion, S. C. Powell, J. S. Stamler, K. N. Houk and E. J. Toone, *J. Am. Chem. Soc.*, 2001, **123**, 8868–8869.
27 P. G. Wang, M. Xian, X. Tang, X. Wu, Z. Wen, T. Cai and A. J. Janczuk, *Chem. Rev.*, 2002, **102**, 1091–1134.
28 C. Baciu and J. W. Gauld, *J. Phys. Chem. A*, 2003, **107**, 9946–9952.
29 Q. K. Timerghazin, G. H. Peslherbe and A. M. English, *Phys. Chem. Chem. Phys.*, 2008, **10**, 1532.
30 D. G. Khomyakov and Q. K. Timerghazin, *J. Chem. Phys.*, 2017, **147**, 044305.
31 L. V. Ivanova, D. Cibich, G. Deye, M. R. Talipov and Q. K. Timerghazin, *ChemBioChem*, 2017, **18**, 726–738.
32 M. R. Talipov, D. G. Khomyakov, M. Xian and Q. K. Timerghazin, *J. Comput. Chem.*, 2013, **34**, 1527–1530.
33 L.-S. Choi and H. Bayley, *Angew. Chemie Int. Ed.*, 2012, **51**, 7972–7976.
34 M. Flister and Q. K. Timerghazin, *J. Phys. Chem. A*, 2014, **118**, 9914–9924.
35 V. Hosseininasab, A. C. McQuilken, A. G. Bakhoda, J. A. Bertke, Q. K. Timerghazin and T. H. Warren, *Angew. Chem. Int. Ed.,* 2020, **59**, DOI:10.1002/anie.202001450.
36 C. Toubin, D. Y.-H. Yeung, A. M. English and G. H. Peslherbe, *J. Am. Chem. Soc.*, 2002, **124**, 14816–14817.
37 E. E. Moran, Q. K. Timerghazin, E. Kwong and A. M. English, *J. Phys. Chem. B*, 2011, **115**, 3112–3126.
38 C. Baciu, K. Cho and J. W. Gauld, *J. Phys. Chem. B*, 2005, **109**, 1334–1336.
39 L. L. Perissinotti, D. A. Estrin, G. Leitus and F. Doctorovich, *J. Am. Chem. Soc.*, 2006, **128**, 2512–2513.
40 L. L. Perissinotti, G. Leitus, L. Shimon, D. Estrin and F. Doctorovich, *Inorg. Chem.*, 2008, **47**, 4723–4733.
41 D. Kazhdan, L. L. Perissinotti, B. Watanabe, M. N. Eberlin, H. M. S. Milagre, B. G. Vaz, D. A. Estrin and F. Doctorovich, *Inorganica Chim. Acta*, 2011, **366**, 85–90.
42 S. Zhang, M. M. Melzer, S. N. Sen, N. Çelebi-Ölçüm and T. H. Warren, *Nat. Chem.*, 2016, **8**, 663–669.
43 S. Tian, J. Liu, R. E. Cowley, P. Hosseinzadeh, N. M. Marshall, Y. Yu, H. Robinson, M. J. Nilges, N. J. Blackburn, E. I. Solomon and Y. Lu, *Nat. Chem.*, 2016, **8**, 670–677.
44 T. Clark, M. Hennemann, J. S. Murray and P. Politzer, *J. Mol. Model.*, 2007, **13**, 291–296.
45 P. Politzer and J. Murray, *Crystals*, 2019, **9**, 165.
46 P. Politzer and J. S. Murray, *Crystals*, 2017, **7**, 212.
47 T. Clark, *Wiley Interdiscip. Rev. Comput. Mol. Sci.*, 2013, **3**, 13–20.
48 M. H. Kolář and P. Hobza, *Chem. Rev.*, 2016, **116**, 5155–5187.
49 G. Cavallo, P. Metrangolo, R. Milani, T. Pilati, A. Priimagi, G. Resnati and G. Terraneo, *Chem. Rev.*, 2016, **116**, 2478–2601.
50 P. Politzer, J. S. Murray and T. Clark, *Phys. Chem. Chem. Phys.*, 2013, **15**, 11178.
51 H. Wang, W. Wang and W. J. Jin, *Chem. Rev.*, 2016, **116**, 5072–5104.
52 G. R. Desiraju, P. Shing Ho, L. Kloo, A. C. Legon, R. Marquardt, P. Metrangolo, P. Politzer, G. Resnati and K. Rissanen, *Pure Appl. Chem*, 2013, **85**, 1711–1713.
53 C. B. Aakeroy, D. L. Bryce, G. R. Desiraju, A. Frontera, A. C. Legon, F. Nicotra, K. Rissanen, S. Scheiner, G. Terraneo, P. Metrangolo and G. Resnati, *Pure Appl. Chem*, 2019, **91**, 1889–1892.
54 B. R. Beno, K. S. Yeung, M. D. Bartberger, L. D. Pennington and N. A. Meanwell, *J. Med. Chem.*, 2015, 58, 4383–4438.
55 L. D. Pennington, M. D. Bartberger, M. D. Croghan, K. L. Andrews, K. S. Ashton, M. P. Bourbeau, J. Chen, S. Chmait, R. Cupples, C. Fotsch, J. Helmering, F.-T. Hong, R. W. Hungate, S. R. Jordan, K. Kong, L. Liu, K. Michelsen, C. Moyer, N. Nishimura, M. H. Norman, A. Reichelt, A. C. Siegmund, G. Sivits, S. Tadesse, C. M. Tegley, G. Van, K. C. Yang, G. Yao, J. Zhang, D. J. Lloyd, C. Hale and D. J. St. Jean, *J. Med. Chem.*, 2015, **58**, 9663–9679.
56 L. A. Hardegger, B. Kuhn, B. Spinnler, L. Anselm, R. Ecabert, M. Stihle, B. Gsell, R. Thoma, J. Diez, J. Benz, J.-M. Plancher, G. Hartmann, D. W. Banner, W. Haap and F. Diederich, *Angew. Chemie Int. Ed.*, 2011, **50**, 314–318.
57 P. S. Ho, *Future Med. Chem.*, 2017, **9**, 637–640.
58 M. R. Scholfield, M. C. Ford, A.-C. C. Carlsson, H. Butta, R. A. Mehl and P. S. Ho, *Biochemistry*, 2017, **56**, 2794–2802.
59 M. C. Ford, M. Saxton and P. S. Ho, *J. Phys. Chem. Lett.*, 2017, **8**, 4246–4252.
60 M. O. Mitchell, *J. Mol. Model.*, 2017, **23**, 287.
61 A. R. Voth, P. Khuu, K. Oishi and P. Shing Ho, *Nat. Chem.*, 2009, **1**, 74–79.
62 B. M. Hudson, E. Nguyen and D. J. Tantillo, *Org. Biomol. Chem.*, 2016, **14**, 3975–3980.
63 D. J. Pascoe, K. B. Ling and S. L. Cockroft, *J. Am. Chem. Soc.*, 2017, **139**, 15160–15167.
64 R. Bertani, P. Sgarbossa, A. Venzo, F. Lelj, M. Amati, G. Resnati, T. Pilati, P. Metrangolo and G. Terraneo, *Coord. Chem. Rev.*, 2010, **254**, 677–695.
65 F. Meyer and P. Dubois, *CrystEngComm*, 2013, **15**, 3058–3071.

66 K. T. Mahmudov, M. N. Kopylovich, M. F. C. Guedes da Silva and A. J. L. Pombeiro, *Dalt. Trans.*, 2017, **46**, 10121–10138.
67 P. Scilabra, G. Terraneo and G. Resnati, *Acc. Chem. Res.*, 2019, **52**, 1313–1324.
68 H. J. Werner, P. J. Knowles, G. Knizia and F. R. Manby, 2012.
69 H. J. Werner, P. J. Knowles, G. Knizia, F. R. Manby and M. Schütz, *Wiley Interdiscip. Rev. Comput. Mol. Sci.*, 2012, **2**, 242–253.
70 T. Shiozaki, G. Knizia and H. J. Werner, *J. Chem. Phys.*, 2011, **134**, 034113.
71 H. J. Werner and P. J. Knowles, *Cit. J. Chem. Phys.*, 1985, **82**, 5803.
72 P. J. Knowles and H. J. Werner, *Chem. Phys. Lett.*, 1985, **115**, 259–267.
73 T. B. Adler and H. J. Werner, *J. Chem. Phys.*, 2011, **135**, 144117.
74 H. J. Werner and K. Pflüger, *Annu. Rep. Comput. Chem.*, 2006, **2**, 53–80.
75 H. J. Werner, T. B. Adler, G. Knizia and F. R. Manby, in *Recent Progress in Coupled Cluster Methods*, Springer Netherlands, Dordrecht, 2010, pp. 573–619.
76 M. Schütz, G. Rauhut and H. J. Werner, *J. Phys. Chem. A*, 1998, **102**, 5997–6003.
77 N. Runeberg, M. Schütz and H. J. Werner, *J. Chem. Phys.*, 1999, **110**, 7210.
78 L. Magnko, M. Schweizer, G. Rauhut, M. Schütz, H. Stoll and H. J. Werner, *Phys. Chem. Chem. Phys.*, 2002, **4**, 1006–1013.
79 O. Masur, D. Usvyat and M. Schütz, *J. Chem. Phys.*, 2013, **139**, 164116.
80 O. Masur, D. Usvyat, M. Schütz, O. Masur and D. Usvyat, *J. Chem. Phys.*, 2013, **139**, 164116.
81 J. P. Perdew, K. Burke and M. Ernzerhof, *Phys. Rev. Lett.*, 1996, **77**, 3865–3868.
82 C. Adamo and V. Barone, *J. Chem. Phys.*, 1999, **110**, 6158.
83 M. Ernzerhof and G. E. Scuseria, *J. Chem. Phys.*, 1999, **110**, 5029.
84 A. E. Reed and F. Weinhold, *J. Chem. Phys.*, 1985, **83**, 1736–1740.
85 D. Feller, *J. Comput. Chem.*, 1996, **17**, 1571–1586.
86 A. D. Becke and E. R. Johnson, *J. Chem. Phys.*, 2005, **123**, 154101.
87 D. J. Frisch, M. J.; Trucks, G. W.; Schlegel, H. B.; Scuseria, G. E.; Robb, M. A.; Cheeseman, J. R.; Scalmani, G.; Barone, V.; Petersson, G. A.; Nakatsuji, H.; Li, X.; Caricato, M.; Marenich, A. V.; Bloino, J.; Janesko, B. G.; Gomperts, R.; Mennucci, B.; Hratch, *Gaussian 16,. Revis. D. 01.*, 2016.
88 F. Weigend and R. Ahlrichs, *Phys. Chem. Chem. Phys.*, 2005, **7**, 3297.
89 D. Rappoport and F. Furche, *J. Chem. Phys.*, 2010, **133**, 134105.
90 E. D. Glendening and F. Weinhold, *J. Comput. Chem.*, 1998, **19**, 593–609.
91 E. D. Glendening, J. K. Badenhoop and F. Weinhold, *J. Comput. Chem.*, 1998, **19**, 628–646.
92 E. D. Glendening, C. Landis and F. Weinhold, *Theor. Chem. Institute, Univ. Wisconsin Madison, WI,* 2018.
93 L. V. Ivanova, B. J. Anton and Q. K. Timerghazin, *Phys. Chem. Chem. Phys.*, 2014, **16**, 8476–8486.
94 We also compared local LCCSD(T)-F12/VDZ-F12 to conventional CCSD(T)-F12/VTZ-F12 on the example of a CH_3SNO-formaldehyde complex (Fig. S2 in ESI). CCSD(T)-F12/VTZ-F12 provides very similar results to LCCSD(T)-F12/VDZ-F12, with a slightly larger binding energy (3.0 kcal/mol vs 2.7 kcal/mol), as expected due to the larger BSSE effects on the conventional coupled-cluster compared to local coupled-cluster calculations.

S-Nitrosothiols, ubiquitous biological derivatives of nitric oxide, can engage in σ-hole/chalcogen bonding with Lewis bases, which, in combination with hydrogen bonding with Lewis acids, could be the basis of enzymatic control of S-nitrosothiol reactions.

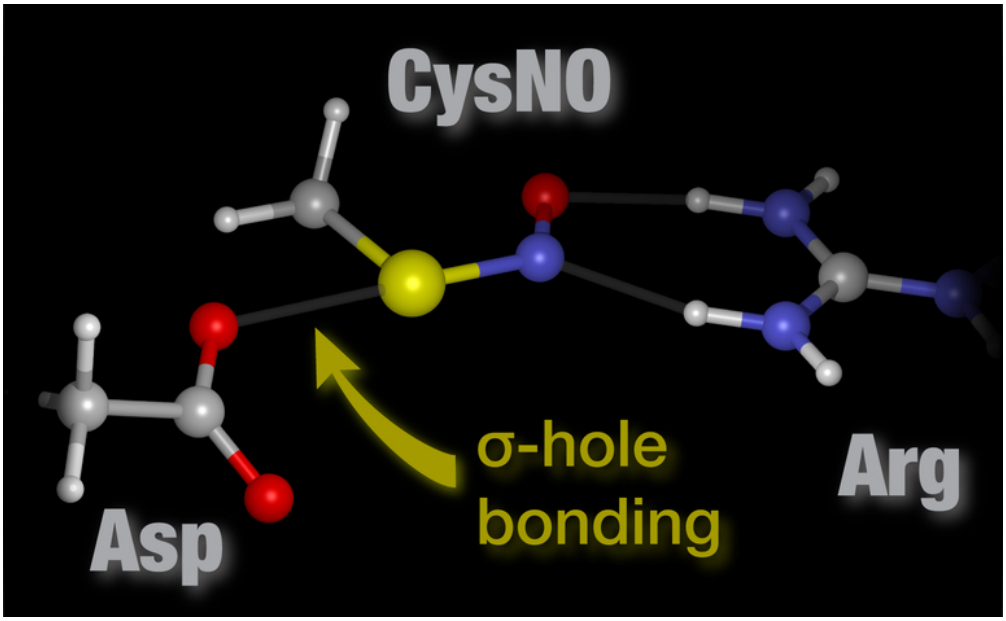

65x40mm (300 x 300 DPI)